Realism of Local and Remote Feedbacks on Tropical Sea Surface Temperatures in Climate Models

Sang-Ik Shin*, Prashant D. Sardeshmukh, and Kathy Pegion

CIRES Climate Diagnostics Center, University of Colorado and NOAA Earth System Research Laboratory, Boulder, Colorado, USA

Journal of Geophysical Research – Atmospheres

(submitted: **Jan. 2010**; revised: **June 2010**)

Abstract

An important emerging issue in climate research is the degree to which a Sea Surface Temperature (SST) change in one tropical ocean basin affects the SST in other basins. In this study the SST interactions among 8 broadly defined regions of coherent SST variability in the tropical Pacific, Indian, and Atlantic oceans are estimated using 3 observational and 76 climate model simulation datasets of the 20th century. The 8-dimensional SST feedback matrix is estimated separately using each dataset by constructing a Linear Inverse Model based on the lag-covariance statistics of the 100-yr monthly SST time series. The simulated feedback matrices are found to differ in several key respects from the observed matrices, and also from one another. In particular, the influence of the eastern Pacific ENSO region on other regions, and of the other regions on the ENSO region, is found to vary considerably from model to model. The representation of remote interactions with the Indo-Pacific Warm Pool region is also found to be

* Current affiliation: College of Marine Science, University of South Florida, 140 7th Ave. S., St. Petersburg, FL.

highly variable. It is argued that these large errors/differences arise mainly from differences in the representation of the remote atmospheric teleconnective feedbacks, and to a lesser extent the local radiative-thermodynamic feedbacks, on the SSTs in the models, whereas differences in the representation of the tropical oceanic wave dynamics are likely less important.

1. Background

Most climate models remain deficient at representing important atmospheric and oceanic aspects of the tropical climate. For example, the simulated atmospheric intertropical convergence zone (ITCZ) varies considerably from model to model, with many models generating an unrealistic "double ITCZ" structure, and in many oceanic simulations a 1-2 K mean SST bias is found over large areas [e.g. Lin 2007]. The ultimate origin of such biases remains a mystery. At least in part, this is because it is still unclear how a change and/or error in one part of the system affects a change and/or error in another part, and what overall effect this has on the simulation and prediction of tropical climate variations.

In this study, we attempt to address the first part of this question. We are especially interested in how the SST variations in the Indian, Pacific, and Atlantic ocean basins are interlinked. Although these basins are separated from each other by the American and African land masses and the Maritime Continent, their interactions with each other, which occur predominantly through the atmosphere on time scales of a few months, can nevertheless be substantial. For example, it is well recognized that El Niño related SST variations in the eastern equatorial Pacific influence climate variability over the adjacent oceans [e.g. Enfield and Mayer 1997;

Penland and Matrosova 1998; Klein et al. 1999; Alexander et al. 2002; Giannini et al. 2004]. Conversely, the relatively weak SST variability in the Indian and Atlantic basins also modifies ENSO variability in the Pacific basin [Yu et al. 2002; Annamalai et al. 2005; Kug and Kang 2006; Kug et al. 2006; Dommenget et al. 2006; Yeh et al. 2007]. The question naturally arises, how accurately do current coupled climate models capture such interactions among these ocean basins?

We are also interested here in the dominant interactions *within* each of these basins, especially between the eastern and western and off-equatorial and equatorial Pacific, between the northern and southern tropical Atlantic, and between the western and eastern Indian oceans. We suspect -- and confirm below -- that these interactions are also not well represented in climate models, partly because (with the possible exception of east-west interactions in the equatorial Pacific) they are not dominated by well-understood oceanic wave dynamics. Even within the equatorial Pacific zone, there are questions concerning how well climate models capture the east-west SST interactions associated with fluctuations of the atmospheric Walker circulation, which are an integral part of the ENSO phenomenon.

Guided by EOF analyses of observed monthly SST variations in each basin (see Figs 1a and 1b), we selected a total of 8 geographically localized regions in the tropics (30°S-30°N) among which to investigate the SST interactions (Fig. 1c). We focused on the *effectively linear feedbacks* among these regions, encapsulated in an 8×8 deterministic system feedback matrix $\mathbf{L}$, by constructing and intercomparing the $\mathbf{L}$ matrices obtained from Linear Inverse Modeling [LIM; see e.g. Penland and Sardeshmukh 1995; Newman et al. 2009] of both observed and simulated

monthly tropical SST variations over the 20th century (1900-1999). We constructed three observationally based **L** matrices using SST datasets compiled at the Hadley Centre of the UK Met Office [HadISST; Rayner et al. 2003], the Lamont-Doherty Earth Observatory [Kaplan et al. 1998], and the National Oceanic and Atmospheric Administration [NOAA; Smith and Raynolds 2005]. We then compared these matrices with 76 **L** matrices derived from 76 coupled model simulations of the 20th century, available at the Program for Climate Model Diagnosis and Intercomparison (PCMDI; http://www-pcmdi.llnl.org). These simulations were generated using prescribed observed time-varying radiative forcings associated with greenhouse gases, aerosols, and solar variations as part of the Climate of the Twentieth Century project (20C3M), as a contribution to the Fourth Assessment Report (AR4) of the Intergovernmental Panel on Climate Change [IPCC 2007]. More details of the simulation and observational datasets used here may be found in the recent paper by Shin and Sardeshmukh (2010), who used identical datasets in their study.

2. Diagnosis method

Our multivariate diagnosis of tropical SST interactions rests on approximating the evolution of tropical variations on longer than weekly time scales by a linear stochastically forced model of the form,

$$\frac{d\mathbf{x}}{dt} = \mathbf{L}\mathbf{x} + \mathbf{B}\eta + \mathbf{F}, \qquad (1)$$

where $\mathbf{x}(t)$ is the N-component system state vector with N=8 components representing the spatially averaged monthly-mean SST anomalies in our 8 regions, all predictable dynamical interactions among the system components are represented in the $N \times N$ deterministic linear feedback matrix $\mathbf{L}$ (sometimes also called the system sensitivity matrix or the matrix of time scales), and all unpredictable chaotic nonlinear dynamics are approximated by the stochastic forcing $\mathbf{B}\eta$, where η is an M-component noise vector of independent white noises and $\mathbf{B}$ is a constant $N \times M$ matrix. Note that the expected mean $\langle \mathbf{B}\eta \rangle$ of this stochastic forcing is zero. The N-component vector $\mathbf{F}$ represents external forcing of the system.

It is important to recognize that although (1) is formulated using only SST, it implicitly includes influences of other climate variables such as winds and ocean currents on SST, and also nonlinear effects, in approximate form. Specifically, deterministic interactions with other variables are implicitly included in $\mathbf{L}$ to the extent that those variables can be linearly diagnosed from the monthly SST anomaly state vector. As for nonlinear effects, the basic premise in (1) concerning the evolution of monthly SST anomalies is that the nonlinear SST tendency terms associated with submonthly SST anomalies and fluxes are in principle linearly parameterizable in terms of the monthly SSTs, and the unparameterized remainder can be treated as stochastic white noise. With these approximations in mind, it is apparent that $\mathbf{L}$ in (1) is not that obtained by directly linearizing the governing fluid dynamical equations but also includes such linear interactions with other variables and linear parameterizations of unresolved processes, and $\mathbf{B}$ accounts for the amplitude and spatial correlation structure of the unparameterized remainder as a "stochastic parameterization". We interpret $\mathbf{L}$ as an *effectively linear feedback matrix* governing monthly SST variations in the tropics. Each of its elements L_{ij} quantifies the direct

dynamical influence (in a dynamical systems sense) of the SST x_j in region *j* on the SST x_i in region *i*, as distinct from additional indirect influences of region *j* on region *i* via other regions *k*. Note that in general $L_{ij} \neq L_{ji}$. Note also that because the system is multivariate, the L_{ij} are not simply identical to the regression coefficients of x_i on x_j.

As discussed in detail by Sardeshmukh and Sura [2009], the relevance of the linear, stochastically forced, approximation (1) in climate system dynamics may be justified using several lines of evidence. First, many coupled climate models are found to respond approximately linearly to imposed GHG and other external radiative forcing changes on decadal and longer timescales [e.g., Meehl et al. 2004; Cash et al. 2005; Knutson et al. 2006 and references therein], consistent with a linear ensemble-mean response $\langle \mathbf{x} \rangle = -\mathbf{L}^{-1}\mathbf{F}$ that one would predict using (1). Second, on shorter interannual scales on which the changes of $\mathbf{F}$ are relatively small, the SST dynamics are consistent with those of a stochastically forced linear system both in the tropics [Penland and Sardeshmukh 1995; Newman et al. 2009] and the extratropics [Hasselmann 1976; Frankignoul 1985; Barsugli and Battisti 1998; Alexander et al. 2008]. Several studies have also shown that the predictable global atmospheric dynamics on these time scales are dominated by linear global responses to tropical SST variations [e.g. Barsugli and Sardeshmukh 2002; Schneider et al. 2003; Barsugli et al. 2006]. Indeed, on these time scales it is difficult to improve upon predictions based on empirical linear correlations, using even state-of-the-art nonlinear dynamical coupled models [e.g. Saha et al. 2006]. The forecast skill of the correlation based models remains competitive with that of comprehensive NWP models even on subseasonal time scales [Winkler et al. 2001; Newman et al. 2003].

Penland and Sardeshmukh [1995, henceforth PS95] and Newman et al. [2009] demonstrated the validity of (1) in tropical SST dynamics through extensive diagnostic and forecasting tests. Their demonstration, conducted in an EOF space, retains its validity in the grid space of interest here because of an attractive property of (1) that it is isomorphic with respect to linear transformations of the state vector $\mathbf{x}$. In other words, if $\mathbf{x}$ evolves according to (1), then a linearly transformed vector $\mathbf{y} = \mathbf{U}\mathbf{x}$ also evolves according to (1), in which $\mathbf{L}$ is replaced by $\mathbf{U}\mathbf{L}\mathbf{U}^{-1}$, $\mathbf{B}$ is replaced by $\mathbf{U}\mathbf{B}$, and $\mathbf{F}$ is replaced by $\mathbf{U}\mathbf{F}$. If $\mathbf{U}$ represents a transformation from grid space to EOF space, then (1) transforms into equations similar to those used and thoroughly tested by PS95 and Newman et al. [2009]. The mapping is not quite 1-to-1 because of the different coarse graining (i.e. truncation) employed in the two representations of (1). Nevertheless, their extensive demonstration of the validity of (1) in tropical SST dynamics is highly relevant in our context. We provide further evidence below that (1) is a good enough approximation for the evolution of monthly SST anomalies on our coarse-grained spatial grid that $\mathbf{L}$ provides useful information on both local and remote SST feedbacks in the tropics.

We used the LIM formalism of PS95 to estimate $\mathbf{L}$ from 3 observational and 76 coupled climate model simulation datasets of the 20th century. The details of LIM may be found in PS95 and are not repeated here. Briefly, $\mathbf{L}$ can be estimated using the lag-covariance equation $\mathbf{C}(\tau) = \exp(\mathbf{L}\tau)\,\mathbf{C}(0)$ satisfied by all dynamical systems of the form (1) with $\mathbf{F} = 0$, where $C_{ij}(\tau) = \langle x_i(t+\tau)\, x_j(t) \rangle$ are the elements of the lag covariance matrix $\mathbf{C}(\tau)$ at time lag τ, by specifying $\mathbf{C}(0)$ and $\mathbf{C}(\tau_0)$ at some lag τ_0. One can repeat this exercise using other training lags τ_0; if the system is indeed of the form (1), then one should obtain the same $\mathbf{L}$. This is the

so-called "Tau test" of PS95 for the validity of linear stochastically forced dynamics. Note that even though $\mathbf{L}$ is estimated using covariances at relatively short lags τ_0 (several months in our case) over which changes of $\mathbf{F}$ are presumed to be negligible, this same $\mathbf{L}$ can then be used to determine the system's response as $\langle \mathbf{x} \rangle = -\mathbf{L}^{-1}\mathbf{F}$ to $\mathbf{F}$ on long time scales.

As mentioned above, our use of LIM here is distinct from that in previous LIM studies [e.g., PS95; Penland and Matrosova 1998; Winkler et al. 2001; Newman et al. 2003; Penland and Matrosova 2006; Alexander et al. 2008; Newman et al. 2009], in which the emphasis was mainly on prediction and predictability, and $\mathbf{L}$ was estimated using observations projected onto a truncated EOF space. Here, our emphasis is on intercomparing the $\mathbf{L}$ matrices estimated from observations and coupled climate model simulations *in grid space*, and to isolate inadequately modeled interactions among specific geographical regions. Such a diagnosis is harder to interpret when performed in a truncated EOF basis, mainly because the dominant EOFs of detrended tropical climate variations are not geographically localized structures and therefore account for different fractions of the SST variance at different locations. Note that we retain *all* of the variance of the detrended area-averaged monthly SST anomalies in each of our 8 regions. The SST anomalies in those regions, obtained after removing the grand mean, mean annual cycle, and linear trend from the 100-yr monthly SST time series, define our 8-component state vector $\mathbf{x}(t)$ in (1).

Despite the seemingly drastic approximations made in (1), estimates of $\mathbf{L}$ from both the observational and simulation SST datasets pass the "Tau test" remarkably well, as shown in Fig. 2. To generate the figure, we estimated $\mathbf{L}$ from each dataset using training lags τ_0 ranging from

1 to at least 5 months. (As explained in PS95, a technical difficulty with LIM is that it fails to estimate $\mathbf{L}$, *even if (1) is valid*, if τ_0 exceeds the half-period corresponding to the highest eigenfrequency of $\mathbf{L}$, i.e. beyond the Nyquist lag). The near-independence of $\mathbf{L}$ on τ_0 may be gauged in Fig. 2 by the nearly constant magnitude of $\mathbf{L}$ times a "representative" constant vector $\underline{\lambda}$ (whose 8 components are proportional to the SST standard deviations in the 8 regions) as τ_0 is varied. The thick black and thin gray curves show the results for $\left|\mathbf{L}\underline{\lambda}\right|$ obtained using the observational and simulation datasets, respectively. It is reassuring that both sets of curves are approximately flat, especially for τ_0 between 1 and 5 months, attesting to the validity of (1). We therefore used throughout this study the average $\mathbf{L}$ matrices obtained for τ_0 ranging from 1 and 5 months. Note, however, that although the observational and model curves in Fig. 2 are approximately flat in this range, the model curves are vertically offset with respect to not only the observational but also other model curves, and also generally terminate at different values of τ_0. These results suggest that the SST feedbacks are indeed effectively linear in both the observations and the models, but the simulated $\mathbf{L}$ matrices differ substantially from the observational matrices and also from one another. These errors and differences are explored in greater detail in the next section.

Before concluding this section, we note that although satisfaction of the "Tau test" is sufficient for establishing the validity of (1), it does not address the question of the relative magnitudes of $\mathbf{Lx}$ and $\mathbf{B}\eta$ in (1), that are closely related to the relative magnitudes of the forecast signal $\exp(\mathbf{L}\tau)\mathbf{x}(t)$ and forecast error ε in the forecast equation $\mathbf{x}(t+\tau) = \exp(\mathbf{L}\tau)\mathbf{x}(t) + \varepsilon$ obtained by integrating (1) (with $\mathbf{F} = 0$) from time t to $t+\tau$. This issue is not directly relevant here, and

as already mentioned, has been investigated in detail in previous LIM studies. Still, one may wonder if our "coarse-graining" of tropical SST variability to 8 degrees of freedom, which is more severe than in the previous LIM studies, significantly distorts some essential aspects of the deterministic (i.e. predictable) tropical SST dynamics, including ENSO dynamics, represented in $\mathbf{L}\mathbf{x}$. Although a detailed predictability analysis is beyond the scope of this study, Fig. 3 provides important reassurance in this regard. It shows the monthly SST forecast anomaly correlation skill, i.e. the correlation of $\exp(\mathbf{L}\tau)\mathbf{x}(t)$ and $\mathbf{x}(t+\tau)$ in each of the i = 1,2,3,..,8 regions for τ = 3, 6, and 9 months over the full 100-yr record, estimated as the square root of $\left[\exp(\mathbf{L}\tau)\mathbf{C}(0)\exp(\mathbf{L}^{\mathrm{T}}\tau)\right]_{ii} \Big/ \left[\mathbf{C}(0)\right]_{ii}$. In essence, this is the ratio of the SST forecast signal standard deviation to the full SST standard deviation. These estimated forecast anomaly correlations are very comparable to those reported in the previous LIM studies of PS95, Newman et al. [2009], and Compo and Sardeshmukh [2010]. In particular, the skill in the ENSO region is just as high as in those studies.

3. Observed and simulated feedback matrices

Equation (1) may be cast in a standardized form by normalizing each component of $\mathbf{x}$ by its standard deviation. The $\mathbf{L}$ matrix then transforms into $\hat{\mathbf{L}} = \mathbf{s}\mathbf{L}\mathbf{s}^{-1}$, where $\mathbf{s}$ is a diagonal matrix of the reciprocals of the SST standard deviations. Note that each element $\hat{L}_{ij}$ of $\hat{\mathbf{L}}$ has units of inverse time (month^{-1} in our case), and thus identifies a characteristic time scale for the influence of an SST anomaly in region j on the anomaly in region i.

Before performing detailed intercomparisons of the $\hat{\mathbf{L}}$ matrices estimated from the 20th century observations and model simulations, we present in Fig. 4 the $\hat{\mathbf{L}}$ matrices estimated using the detrended monthly SST anomaly fields for all of the 20th century, and for just the first and second halves of the century, from the three observational SST datasets (HadISST, Kaplan, and NOAA). We do this not only to provide observational targets for the $\hat{\mathbf{L}}$ matrices derived from the 20th century model simulations, but also to gain a sense of the "fuzziness" in those targets associated with dataset dependence and sampling uncertainty. It should be noted, however, that the differences between the $\hat{\mathbf{L}}$ matrices derived from the data for the first and second halves of the 20th century are indicative not only of sampling uncertainty; they also include a contribution from real 20th century climate change. Given also that the sampling uncertainty in the 100-yr $\hat{\mathbf{L}}$ estimates is smaller than in the 50-yr estimates, we interpret the differences between the first and second 50-yr $\hat{\mathbf{L}}$ estimates as providing rough upper bounds on the sampling uncertainty in the 100-yr $\hat{\mathbf{L}}$ estimates, which we used in all our comparisons with the $\hat{\mathbf{L}}$ estimates from the 100-yr model simulations.

Despite the above caveats, there is a reassuring consistency among the 9 observational estimates of each element $\hat{L}_{ij}$ of $\hat{\mathbf{L}}$ in Fig. 4, except for the estimate based on the first half-century HadISST data, which is an outlier in many instances. Not surprisingly, the consistency among the three datasets tends to be high for $\hat{L}_{ij}$ estimated from the data-rich second half-century record, and low for $\hat{L}_{ij}$ estimated from the data-poor first half-century record. Fortunately, the 100-yr $\hat{L}_{ij}$ estimates are much more consistent among the 3 datasets than the first half-century estimates, and in most cases they are nearly as consistent as the second-half century estimates.

Figure 5 provides a detailed intercomparison of the observed and simulated 100-yr $\hat{\mathbf{L}}$ matrices. At each (*i*,*j*) location on the plot, the gray horizontal line segments show estimates of $\hat{L}_{ij}$ from the 76 individual model simulations. The range of the corresponding 3 observational $\hat{L}_{ij}$ estimates is indicated by the width of the red rectangle below the horizontal axis. The multi-model ensemble mean of $\hat{L}_{ij}$ is also shown below the horizontal axis as a filled blue circle, together with two different measures of simulated uncertainty: the multi-model ensemble spread of $\hat{L}_{ij}$ ($\pm \sigma_{\mathrm{ALL}}$; outer blue bars), and the average of the "internal" ensemble spread obtained for specific models with at least 3 ensemble members[1] ($\pm \sigma_{\mathrm{INT}}$; shorter inner blue bars). In essence, σ_{INT} is a measure of the consistency of $\hat{L}_{ij}$ estimated using different simulations of the same model. The fact that σ_{INT} is generally much smaller than σ_{ALL} in Fig. 5 suggests that most of the multi-model spread of the $\hat{L}_{ij}$ estimates arises from actual model differences, rather than sampling error.

Figure 5 shows that to a first approximation, monthly SST anomalies throughout the tropics are strongly damped by local interactions within the air-sea column, as indicated by the predominantly negative values of the diagonal elements $\hat{L}_{ii}$ of $\hat{\mathbf{L}}$ in both observations and models. (Note that the scale for the diagonal elements in the figure is twice that for the off-diagonal elements). This local damping time scale is relatively short (~ 4 months) in the Indian and Western Pacific (Regions 1-3), somewhat longer (~ 6 months) in the Atlantic (Regions 7-8),

[1] In clustering the coupled models, different versions of a model (including different resolution versions) from the same modeling group were treated separately. We determined a total of 14 such distinct model clusters. They are indicated by the right-handed brackets at the far right edge of the plot.

and relatively long (6 to 9 months) in the eastern Pacific (Regions 4-6) basins. It is longest in the Cold Tongue "ENSO" region of the eastern equatorial Pacific (Region 5). The multi-model ensemble mean values of $\hat{L}_{ii}$ are generally in reasonable agreement with the observed values, although there is considerable inter-model spread that is largest (relative to the ensemble-mean value) in the ENSO Region 5. The positive bias of the models' $\hat{L}_{55}$ with respect to the observed (indicative of weaker than observed local damping) is also relatively the largest. A similar weak local damping bias was implicated by Sun et al. [2006] in the excessive coldness of the long-term mean SSTs in this region in a smaller group of coupled model simulations. Apparently the spuriously weak damping of SSTs in the ENSO region remains a prevalent problem.

Given the importance of ENSO, the remote influence on the ENSO region from other regions ($\hat{L}_{5j}$), as well as the influence *of* the ENSO region on the other regions ($\hat{L}_{i5}$) are of particular interest. These interactions are highlighted by the green and yellow colored 5th row and 5th column, respectively, of $\hat{L}$ in Fig. 5. Significant model misrepresentations of the remote impacts on the ENSO region ($\hat{L}_{5j}$) are evident, consistent with the suggestion from previous studies that simulation errors outside the Pacific basin also contribute substantially to errors in ENSO simulations [e.g. Guilyardi et al. 2009]. For instance, the damping impact of Indian Ocean SSTs on ENSO suggested in many studies [e.g. Annamalai et al. 2005; Kug and Kang 2006; Kug et al. 2006; Dommenget et al. 2006; Yeh et al. 2007] is clear in both our observational and model based $\hat{L}_{5j}$ estimates; however, the exact locations of the influential regions are different. Whereas the models are in unanimous agreement that the damping influence is exerted from the entire Indian ocean basin, the observations show a strong damping influence only from the

eastern half of the basin (see also $\hat{L}_{51}$ and $\hat{L}_{52}$ in Fig. 4). The models also misrepresent the influence of the Atlantic SSTs on ENSO. The observations suggest a very weak influence, whereas the models suggest a substantial influence, but with little inter-model agreement even with regard to the sign of the North Atlantic influence ($\hat{L}_{57}$). And finally, Fig. 5 provides evidence that the influence of the northern off-equatorial SSTs on the equatorial SSTs in Region 5 ($\hat{L}_{54}$) is systematically too strong in the models compared to observations.

Some aspects of the impact of SSTs in the ENSO region on other regions ($\hat{L}_{i5}$) are also not well captured by the coupled models. For instance, the impacts on the eastern Indian ($\hat{L}_{25}$) and southern tropical Atlantic oceans ($\hat{L}_{85}$) are clearly outside the range of the observational estimates. Also, there is strong inter-model disagreement concerning even the sign of the impact on the Warm Pool SSTs ($\hat{L}_{25}$, $\hat{L}_{35}$). With regard to the impact on SSTs in the regions to the immediate north and south of the ENSO region, the models suggest a large positive impact on both regions ($\hat{L}_{45} > 0$ and $\hat{L}_{65} > 0$), whereas the observations suggest a large impact only on southern region ($\hat{L}_{65} > 0$).

Besides interactions with the ENSO region, Fig. 5 suggests significant model misrepresentations of the Indian ocean influences on the southern Atlantic basin ($\hat{L}_{81}$ and $\hat{L}_{82}$); the western Pacific influences on the Eastern Indian ($\hat{L}_{23}$), northeastern Pacific ($\hat{L}_{43}$), southeastern Pacific ($\hat{L}_{63}$) and southern Atlantic ($\hat{L}_{83}$) basins; the northeastern Pacific influence on the western Pacific ($\hat{L}_{34}$) basin; and the northern Atlantic influence on the western Indian ($\hat{L}_{17}$) and northeastern and

southeastern Pacific ($\hat{L}_{47}$ and $\hat{L}_{67}$) basins. In several instances these influences are inconsistent even with regard to sign among the models.

4. Summary and discussion

In this study we investigated the interactions among 8 broadly defined regions of coherent tropical SST variability in the Pacific, Indian, and Atlantic Ocean basins using 3 observational and 76 climate model simulation datasets of the 20th century. The 8-dimensional SST feedback matrix was estimated separately using each dataset by constructing a Linear Inverse Model based on the lag-covariance statistics of the 100-yr monthly SST time series. In general, we found the local feedbacks on SST in our 8 selected regions to be reasonably consistent among the observations and the coupled models, although relatively less so in the eastern equatorial ENSO region (Region 5). It was in the representation of the *remote* feedbacks that we found the models to differ most from the observations, and also from one another. In particular, we found the influence of the eastern Pacific ENSO region on other regions, and of the other regions on the ENSO region, to vary considerably from model to model. We also found the representation of remote interactions with the Indo-Pacific Warm Pool region to be highly variable.

Figure 5 provides a comprehensive summary of the results from our local and remote feedback analysis. It depicts the realism or otherwise of coupled model representations of all possible interactions among our 8 selected regions of dominant tropical SST variability. Although our emphasis was on highlighting those interactions that are represented particularly poorly in the models, the figure gives an impression of large inter-model inconsistencies in the remote

feedbacks even in instances when the multi-model ensemble-mean feedback is in reasonable agreement with the observations.

Given such model errors and inconsistencies in the feedback operator $\mathbf{L}$, relying on any one particular climate model to generate realistic responses $\langle \mathbf{x} \rangle = -\mathbf{L}^{-1}\mathbf{F}$ to external forcing is clearly unjustified. Focusing on the multi-model ensemble mean response $\overline{\langle \mathbf{x} \rangle} = -\overline{\mathbf{L}^{-1}}\mathbf{F}$ is the usual suggested solution to this problem. However, we have provided evidence that even the multi-model mean operator $\overline{\mathbf{L}}$ differs from the observed operator in several key respects. The conclusion seems inescapable that at the very least, some important elements of $\overline{\mathbf{L}}$ highlighted in this paper should agree better with the observations to increase our confidence in the ability of even an ensemble of models to generate reliable responses to external forcing. Reduction of interaction errors that are systematic across all the models in Fig. 5 would appear to be an obvious first area of focus. The fact that such interactions, especially among the basins separated by continental land masses, generally occur on time scales of a few months at most suggests that they occur primarily through the atmosphere and not through the oceans, which should help in error diagnosis and reduction.

We end by noting to an encouraging aspect of isolating model errors at the level of the feedback operator $\mathbf{L}$, as done here, as opposed to merely documenting long-term simulation errors to demonstrate the existence of model errors. This is that the model errors in $\mathbf{L}$ should be manifested in errors of tropical SST forecasts made using the models even at short forecast ranges of, say, three months given the validity of (1) even at these short ranges as demonstrated in Figs. 2 and 3. This suggests that an extensive model improvement program involving very

large numbers of short experimental model integrations to diagnose and reduce the short-range SST forecast errors and, concurrently, the errors in $\mathbf{L}$ might be fruitful.

Acknowledgments. This work was supported by a grant from NOAA's Climate Variability and Predictability (CVP) Program.

References

Alexander, M. A., I. Blade, M. Newman, J. R. Lanzante, N.-C. Lau, and J. D. Scott (2002), The atmospheric bridge: The influence of ENSO teleconnections on air-sea Interaction over the global oceans, *J. Climate*, *15*, 2205-2231.

Alexander, M. A., L. Matrosova, C. Penland, J. D. Scott, and P. Chang (2008), Forecasting pacific SSTs: Linear Inverse Model predictions of the PDO, *J. Climate*, *21*, 385-402.

Annamalai, H., S. P. Xie, J. P. McCreary, and R. Murtugudde (2005), Impact of Indian Ocean sea surface temperature on developing El Niño, *J. Climate*, *18*, 302-319.

Barsugli J. J., and D. S. Battisti (1998), The basic effects of atmosphere–ocean thermal coupling on midlatitude variability, *J. Atmos. Sci.*, *55*, 477–493.

Barsugli. J. J., and P. D. Sardeshmukh (2002), Global atmospheric sensitivity to tropical SST anomalies throughout the Indo-Pacific Basin, *J. Climate*, *15*, 3427-3442.

Barsugli J. J., S.-I. Shin, and P. D. Sardeshmukh (2006), Sensitivity of global warming to the pattern of tropical ocean warming, *Clim. Dyn.*, *27*, 483-492.

Cash, B. A., E. K. Schneider, and L. Bengtsson (2005), Origin of regional climate differences: role of boundary conditions and model formulation in two GCMs, *Clim. Dyn.*, *25*, 709-723.

Compo, G. P., and P. D. Sardeshmukh (2010), Removing ENSO-related variations from the climate record, *J. Climate*, *23*, 1957-1978.

Dommenget, D., V. Semenov, and M. Latif (2006), Impacts of the tropical Indian and Atlantic Oceans on ENSO, *Geophys. Res. Lett.*, *33*, L11701, doi:10.1029/2006GL025871.

Enfield, D. B., and D. A. Mayer (1997), Tropical Atlantic sea surface temperature variability and its relation to El Niño-Southern Oscillation, *J. Geophys. Res.*, 102, 929– 946.

Frankignoul, C. (1985), Sea surface temperature anomalies, planetary waves, and air-sea feedback in the middle latitudes, *Rev. Geophys., 23*, 357–390.

Giannini, A., R. Saravanan, and P. Chang (2004), The preconditioning role of Tropical Atlantic variability in the development of the ENSO teleconnection: Implications for the prediction of Nordeste rainfall. *Clim. Dyn., 22*, 839-855.

Guilyardi, E., and Coauthors (2009), Understanding El Niño in ocean-atmosphere general circulation models: Progress and challenges, *Bull. Amer. Meteor. Soc.*, *90*, 325-340.

Hasselmann, K. (1976), Stochastic climate models. Part I. Theory, *Tellus, 28*, 473–484.

IPCC (2007), Climate Change 2007: The Physical Science Basis. Contribution of Working Group I to the Fourth Assessment Report of the Intergovernmental Panel on Climate Change [Solomon, S., D. Qin, M. Manning, Z. Chen, M. Marquis, K. B. Averyt, M. Tignor, and H. L. Miller (eds.)], Cambridge University Press, Cambridge, United Kingdom and New York, pp. 996.

Kaplan, A., M. Cane, Y. Kushnir, A. Clement, M. Blumenthal, and B. Rajagopalan (1998), Analyses of global sea surface temperature 1856-1991, *J. Geophys. Res.*, *103*, 18567-18589.

Klein, S. A., Soden, B. J., and N.-C. Lau (1999), Remote sea surface temperature variations during ENSO: Evidence for a tropical atmospheric bridge, *J. Climate*, *12*, 917-932.

Knutson, T. R., and Coauthors (2006), Assessment of Twentieth-Century regional surface temperature trends using the GFDL CM2 coupled models, *J. Climate*, *19*, 1624-1651.

Kug, J. S., and I. S. Kang (2006), Interactive Feedback between ENSO and the Indian Ocean. *J. Climate*, *19*, 1784–1801.

Kug, J. S., Kirtman, B. P., and I. S. Kang (2006), Interactive Feedback between ENSO and the Indian Ocean in an Interactive Ensemble Coupled Model. *J. Climate, 19,* 6371–6381.

Lin, J. L. (2007), The double-ITCZ problem in IPCC AR4 coupled GCMs: Ocean-atmosphere feedback analysis, *J. Climate*, *20*, 4497-4525.

Meehl, G. A., W. M. Washington, J. M. Arblaster, and A. Hu (2004), Factors affecting climate sensitivity in coupled models, *J. Climate*, *17,* 1584-1596.

Newman, M., P. D. Sardeshmukh, C. R. Winkler, and J. S. Whitaker (2003), A study of subseasonal predictability, *Mon. Wea. Rev.*, *131,* 1715-1732.

Newman, M., P. D. Sardeshmukh, and C. Penland (2009), How important is air-sea coupling in ENSO and MJO evolution? *J. Climate*, *22*, 2958-2977.

Penland, C., and P. D. Sardeshmukh (1995), The optimal growth of tropical sea surface temperature anomalies, *J. Climate*, *8*, 1999-2024.

Penland, C., and L. Matrosova (1998), Prediction of tropical Atlantic sea surface temperatures using Linear Inverse Modeling, *J. Climate*, *11*, 483-496.

Penland, C., and L. Matrosova (2006), Studies of El Nino and interdecadal variability in tropical sea surface temperatures using a nonnormal filter, *J. Climate*, *19*, 5796-5815.

Rayner, N. A., and Coauthors (2003), Global analyses of sea surface temperature, sea ice, and night marine air temperature since the late nineteenth century, *J. Geophys. Res.*, *108*, 4407, doi:10.1029/2002JD002670.

Saha, S., and Coauthors (2006), The NCEP Climate Forecast System, *J. Climate*, *19*, 3483-3517.

Sardeshmukh, P. D., and P. Sura (2009) Reconciling non-Gaussian climate statistics with linear dynamics, *J. Climate*, *22*, 1193-1207.

Schneider, E. K., L. Bengtsson, and Z.-Z. Hu (2003), Forcing of Northern Hemisphere climate

trends, *J. Atmos. Sci.*, *60*, 1504-1521.

Shin, S.-I., and P. D. Sardeshmukh (2010) Critical influence of the pattern of tropical ocean warming on remote climate trends, *Clim. Dyn.*, DOI:10.1007/s00382-009-0732-3.

Smith T. M. and R. W. Raynolds (2005), A global merged land-air-sea surface temperature reconstruction based on historical observations (1880-1997), *J. Climate*, *18*, 2021-2036.

Sun, D.-Z., T. Zhang, C. Covey, S. Klein, W. D. Collins, J. J. Hack, J. T. Kiehl, G. A. Meehl, I. M. Held, and M. Suarez (2006), Radiative and dynamical feedbacks over the equatorial cold-tongue: Results from nine atmospheric GCMs, *J. Climate* , *19*, 4059-4074.

Winkler, C. R., Newman,M., and P. D. Sardeshmukh (2001), A linear model of wintertime low-frequency variability. Part I: Formulation and forecast skill, *J. Climate*, *14*, 4474-4494.

Yeh, S.-W., R. Wu, and B. P. Kirtman (2007), Impact of the Indian Ocean on ENSO variability in a hybrid coupled model, *Q. J. R. Meteorol. Soc.*, *133*, 445-457.

Yu, J.-Y., C. R. Mechoso, J. C. McWilliams, and A. Arakawa (2002), Impacts of the Indian Ocean on the ENSO cycle, *Geophys. Res. Lett.*, *29*, 1204, doi:10.1029/2001GL014098.

Figure Legends

Fig. 1 (a) The dominant regional EOFs of monthly SST anomalies in the tropical Indian, Pacific, and Atlantic Oceans obtained from separate EOF analyses and shown in the same map for ease of presentation. The regional boundaries of the EOF analyses are indicated by thick black lines. The numbers along bottom indicate the fractional variance explained by the EOFs. (b) As in (a) but for the second most dominant EOFs. The SST data are from the 20th century (1900-1999) HadISST data set [Rayner et al. 2003]. The data were interpolated to a T42 Gaussian grid before performing the EOF analyses. The raw EOF patterns obtained were then spatially smoothed using a T21 spectral filter to emphasize the large-scale features. (c) Our 8 selected tropical regions of geographically coherent SST variability based upon the EOF analyses: Region 1: WTI (Western Tropical Indian), Region 2: ETI (Eastern Tropical Indian), Region 3: WTP (Western Tropical Pacific), Region 4: NSP (North Subtropical Pacific), Region 5: ENSO, Region 6: SSP (South Subtropical Pacific), Region 7: NTA (North Tropical Atlantic), and Region 8: STA (South Tropical Atlantic).

Fig. 2 The dependence of the magnitude $\left|\mathbf{L}\underline{\lambda}\right|$ of the effective SST feedback matrix $\mathbf{L}$ times a "representative" constant vector $\underline{\lambda}$, on the training lag τ_0 used for estimating $\mathbf{L}$. Results are shown for $\mathbf{L}$ estimated using 3 observational (thick black curves) and 76-coupled simulation (thin gray curves) datasets. Note that although the model results differ substantially from the tightly clustered observational results, the curves for both observations and models are approximately flat for τ_0 between 1 and 5 months (demarcated by light gray shading).

Fig. 3 The estimated correlation of predicted and observed area-averaged monthly tropical SST anomalies in the 8 tropical regions of interest, at forecast lead times of 3, 6, and 9 months. The correlation is estimated as the ratio of the standard deviations of the predicted and observed monthly SST anomalies over the 20th century (1900-1999). Results obtained using the HadISST (solid black bars), Kaplan (grey bars), and NOAA (white bars) SST datasets are shown separately. See text for more explanation.

Fig. 4 The elements $\hat{L}_{ij}$ of the standardized 8×8 effective linear SST feedback matrix $\hat{\mathbf{L}}$ (units: month^{-1}) estimated using detrended observed monthly SST anomaly fields for the full 20th century (red symbols), and also estimated using the SST fields for only the first 50 years (green symbols) and last 50 years (blue symbols) of the 100-yr period. For each matrix element (*i*,*j*) the sets of upper circles, middle triangles, and lower squares show the $\hat{L}_{ij}$ values (along the horizontal axis, i.e. as the distance from the vertical line segment) estimated using, respectively, the HadISST, Kaplan, and NOAA SST datasets. The results for the diagonal elements are highlighted within large grey shaded squares. Note that the scale for the diagonal elements is twice that for the off-diagonal elements, as indicated in the upper left corner of the plot. See text for further details.

Fig. 5 Intercomparisons of the elements of the standardized 8×8 effective linear SST feedback matrix $\hat{\mathbf{L}}$ (units: month^{-1}) estimated using 3 observational and 76 climate model simulation datasets. Note that the scale for the diagonal elements in the figure is twice that for the off-diagonal elements. For each matrix element (*i*,*j*), the gray bars show $\hat{L}_{ij}$ estimated using the 76 individual simulations. The multi-model ensemble mean $\hat{L}_{ij}$ is indicated by the blue dot below

the horizontal axis, along with the multi-model ensemble spread of $\hat{L}_{ij}$ among all 76 simulations ($\pm\sigma_{\mathrm{ALL}}$; large outer blue bars), and the average of the internal ensemble spread of $\hat{L}_{ij}$ obtained in 14 subsets of the ensemble simulations, each containing at least 3 ensemble members, generated using distinct models ($\pm\sigma_{\mathrm{INT}}$; smaller inner blue bars). These 14 simulation subsets are indicated by the right-handed brackets at the far right edge of the plot. The range of the $\hat{L}_{ij}$ values estimated using the 3 observational datasets is indicated by the width of the red rectangles below the horizontal axis. $\hat{L}_{ij}$ is a measure of the direct influence of the standardized SST anomalies in region *j* on the standardized SST anomalies in region *i* (see Fig. 1 for locations). The influences on the equatorial eastern Pacific "ENSO" Region 5 from the other regions ($\hat{L}_{5j}$), and the influences *of* the ENSO region on the other regions ($\hat{L}_{i5}$), are highlighted by the green colored 5$^{\mathrm{th}}$ row and yellow colored 5$^{\mathrm{th}}$ column, respectively, of $\hat{\mathbf{L}}$. See text for further details.

a) Regional EOF-1

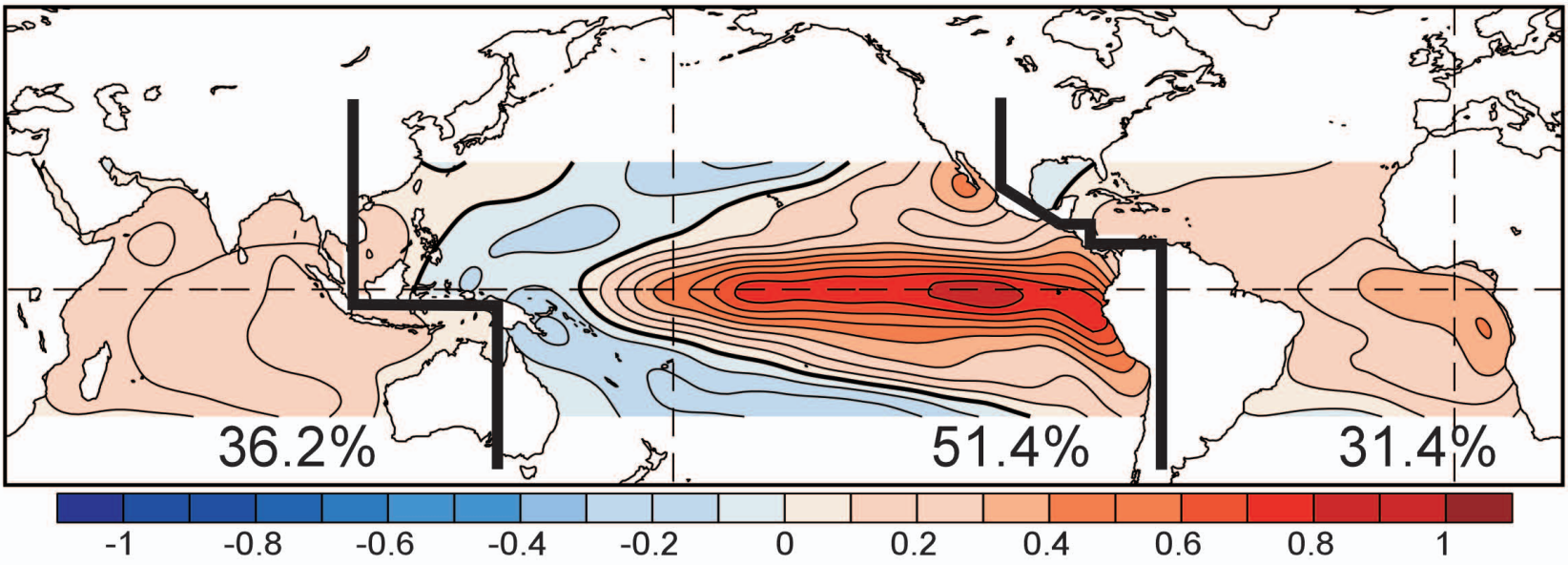

b) Regional EOF-2

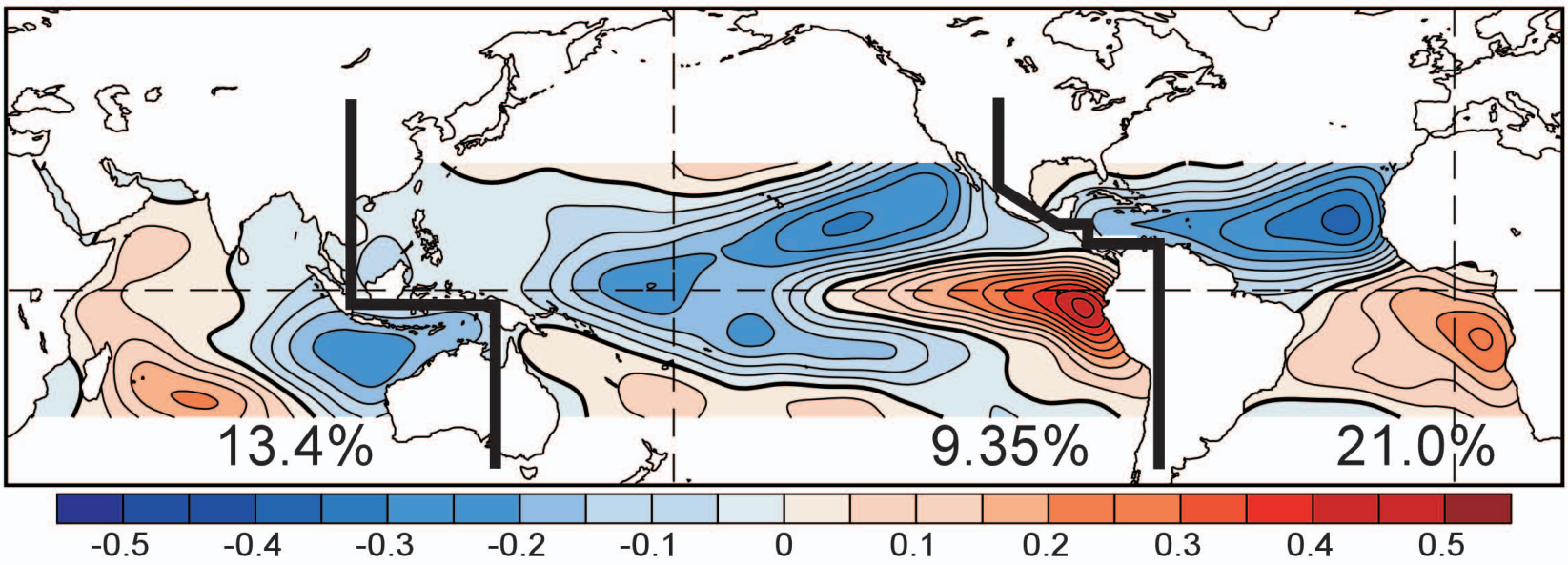

c) Regional Mask

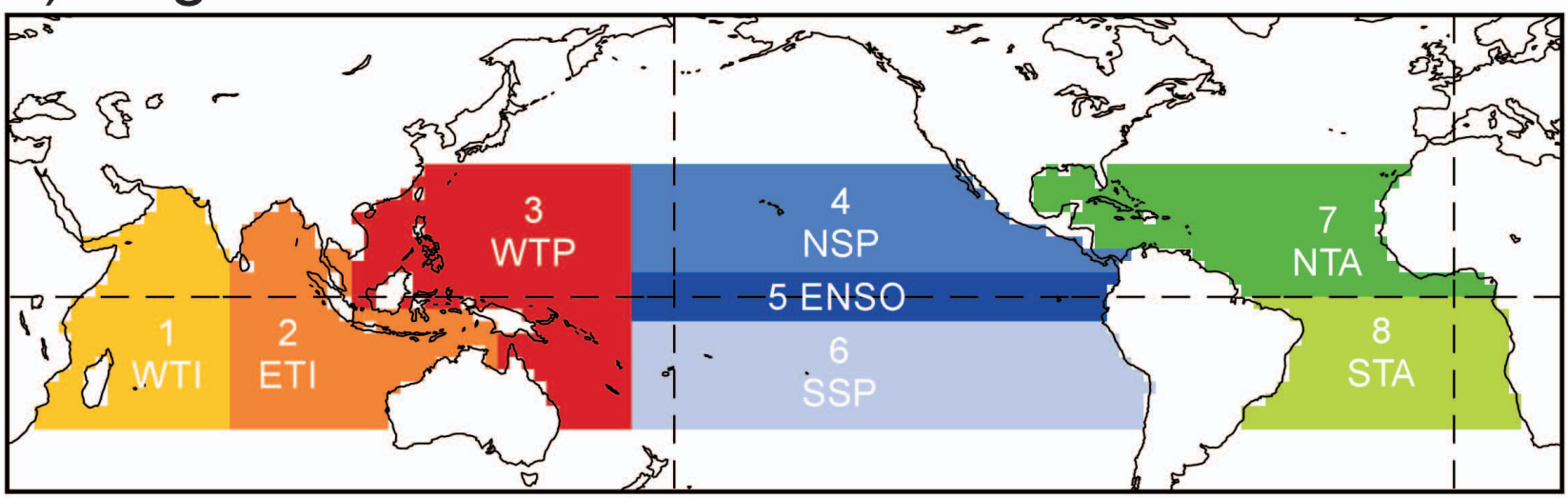

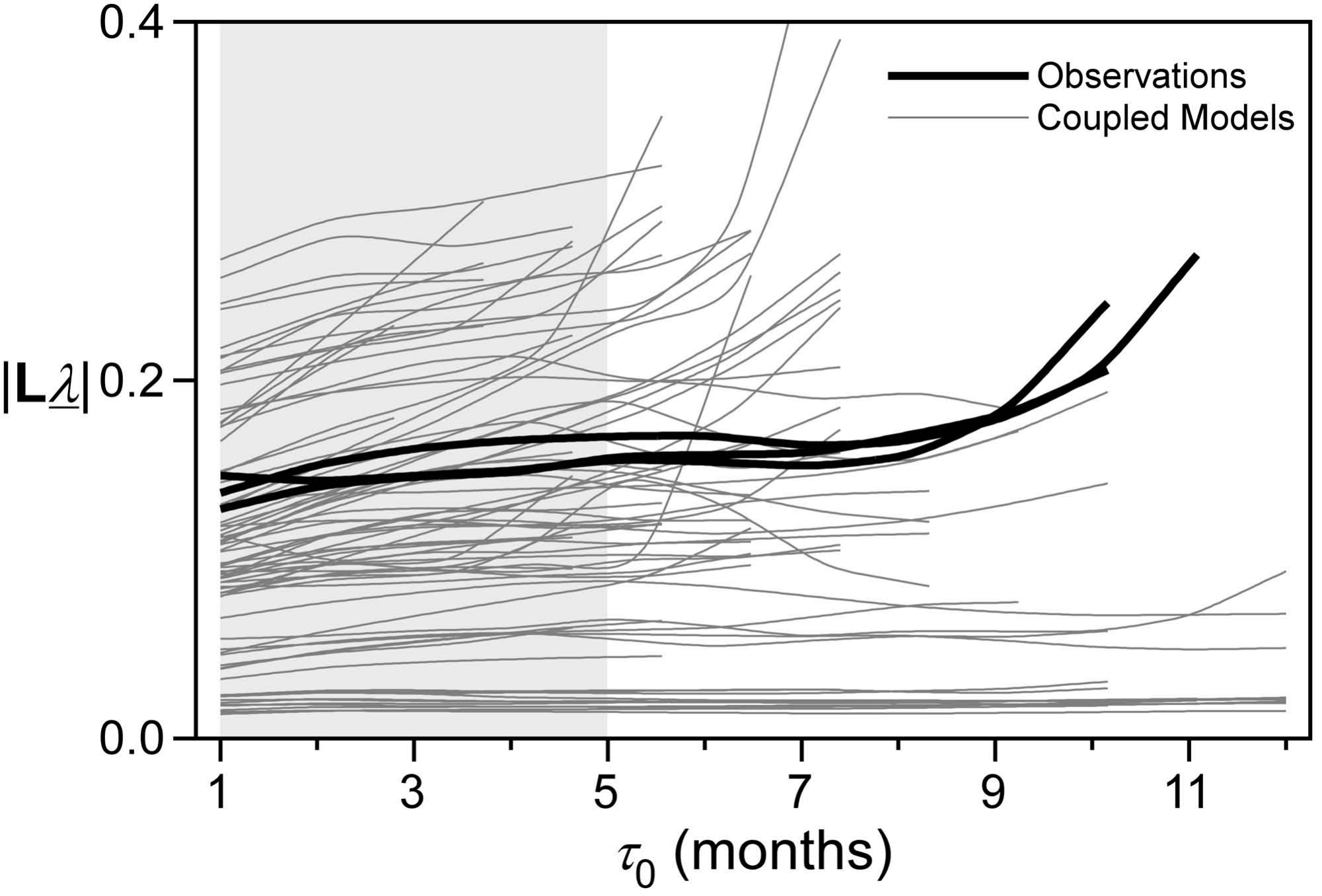
0.4
0.2
0.0
|L$\underline{\lambda}$|
Observations
Coupled Models
1
3
5
7
9
11
τ_0 (months)

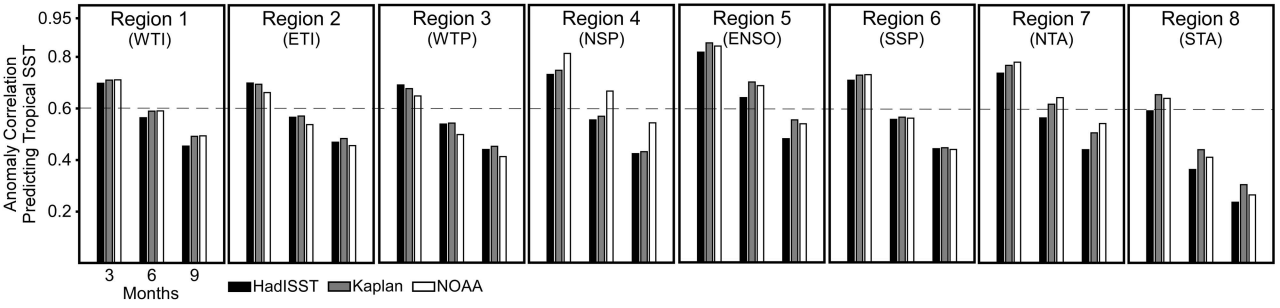
Region 1
(WTI)
Region 2
(ETI)
Region 3
(WTP)
Region 4
(NSP)
Region 5
(ENSO)
Region 6
(SSP)
Region 7
(NTA)
Region 8
(STA)
Anomaly Correlation
Predicting Tropical SST
0.95
0.8
0.6
0.4
0.2
3
6
9
Months
HadISST
Kaplan
NOAA

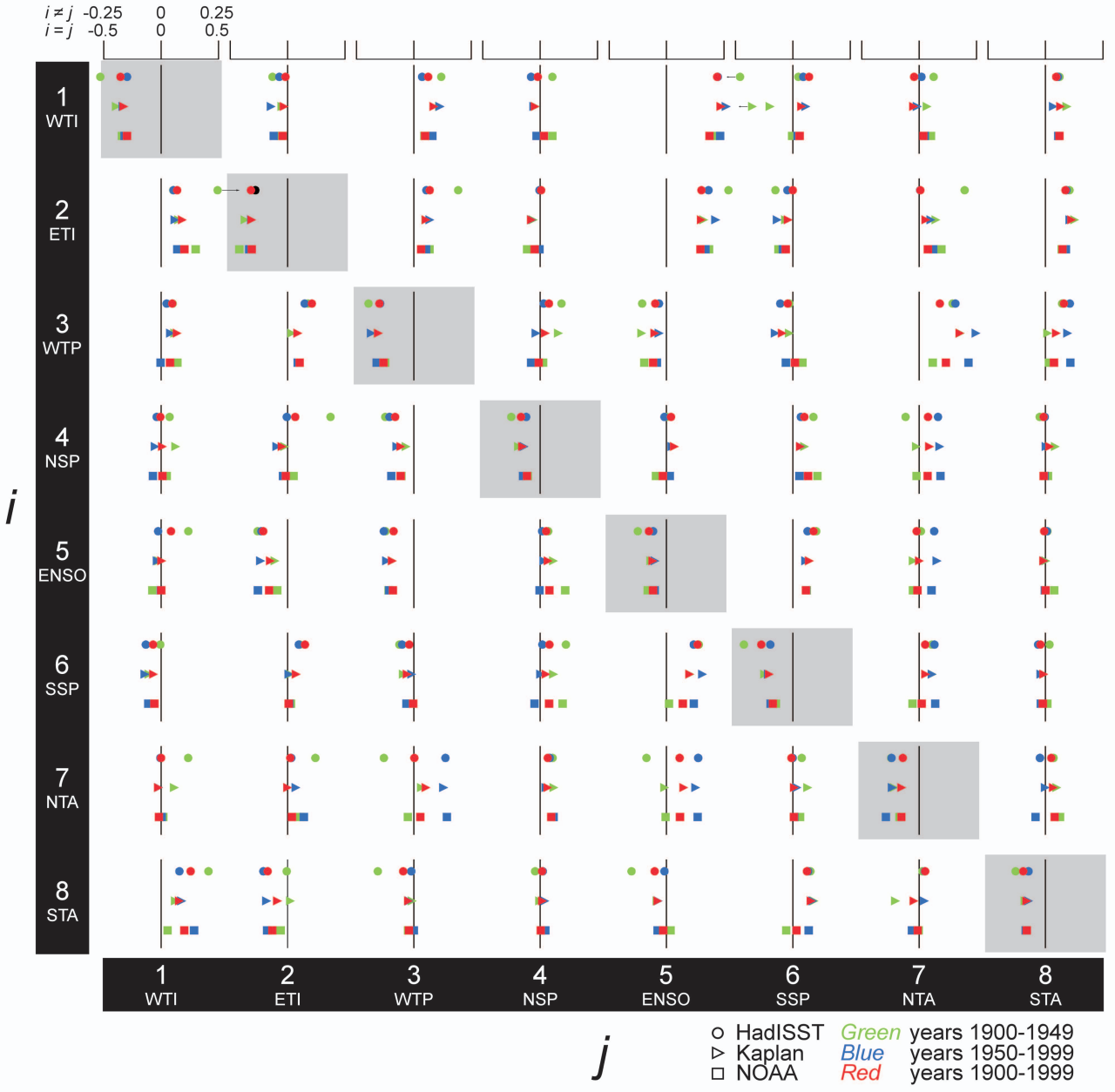
i ≠ j -0.25 0 0.25
i = j -0.5 0 0.5
1 WTI
2 ETI
3 WTP
4 NSP
5 ENSO
6 SSP
7 NTA
8 STA
i
1 WTI
2 ETI
3 WTP
4 NSP
5 ENSO
6 SSP
7 NTA
8 STA
j
HadISST Green years 1900-1949
Kaplan Blue years 1950-1999
NOAA Red years 1900-1999

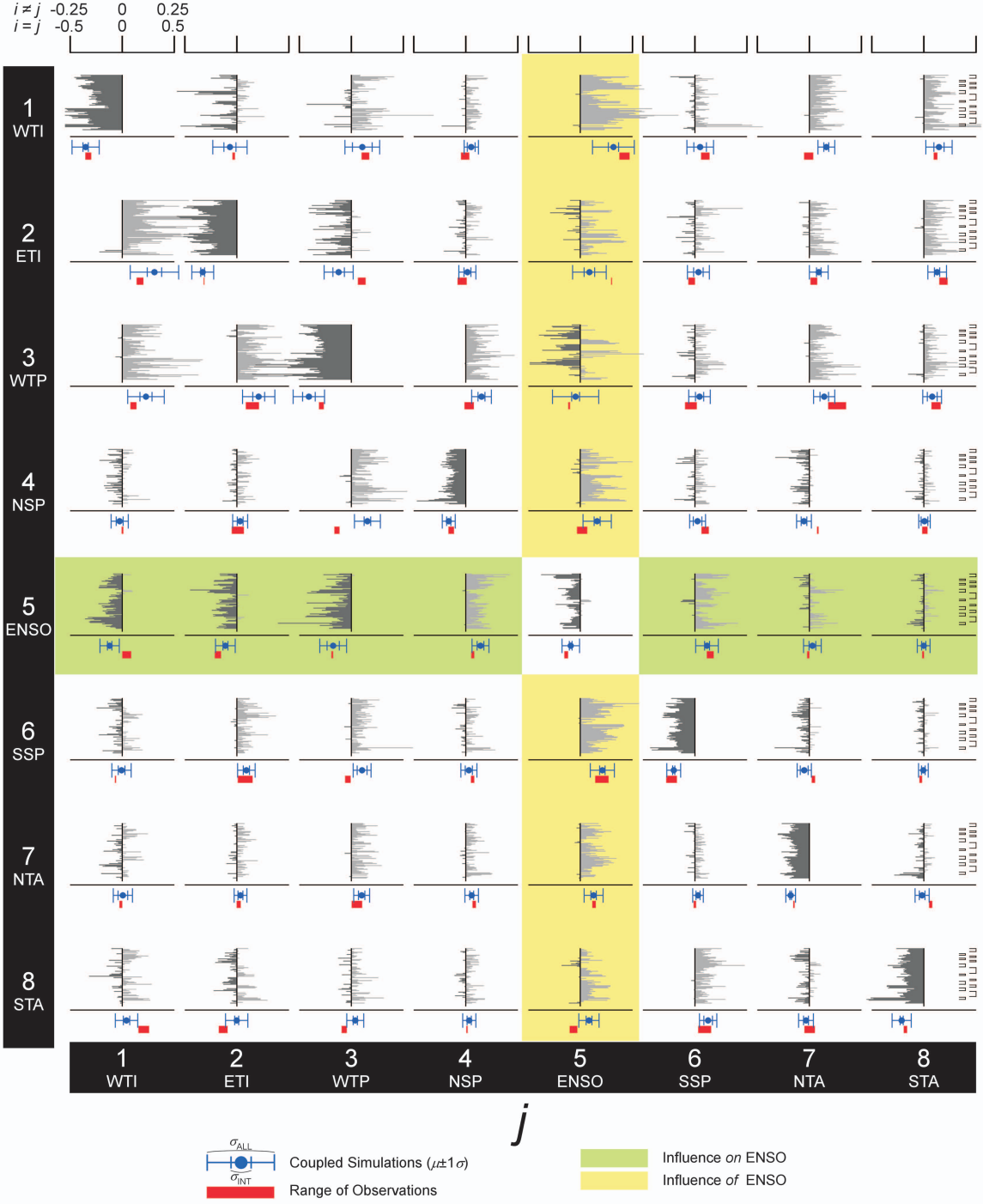
i ≠ j -0.25 0 0.25
i = j -0.5 0 0.5
1 WTI
2 ETI
3 WTP
4 NSP
5 ENSO
6 SSP
7 NTA
8 STA
i
1 WTI
2 ETI
3 WTP
4 NSP
5 ENSO
6 SSP
7 NTA
8 STA
j
σALL
σINT
Coupled Simulations (μ±1σ)
Range of Observations
Influence on ENSO
Influence of ENSO